Antialiasing Filtering for Projection-based Light Field Displays

Kamran Akbar
Tampere University
Tampere, Finland
kamran.akbar@tuni.fi

Robert Bregovic
Tampere University
Tampere, Finland
robert.bregovic@tuni.fi

***Abstract* – Projection-based light field displays can achieve realistic visualization of a 3D scene. However, these displays can reproduce only a finite number of light rays, thus their bandwidth is limited in terms of angular and spatial resolution. Consequently, a display cannot show parts of the 3D scene that falls outside of its bandwidth region without aliasing distortion. Therefore, light fields should be properly pre-processed before visualizing them on a light field display. In this paper, we develop two methods for designing antialiasing filters that will either remove or blur parts of the scene in the input light field that causes aliasing. We illustrate the effectiveness of the proposed methods by comparing the visualized light fields on a projection-based light field display before and after applying the designed antialiasing filters.**

***Keywords* — light field, antialiasing filter, projection-based light field display, epipolar plane image**

I. INTRODUCTION

The available 3D displays, such as stereoscopic displays, (super) multi-view displays, and light field displays, can realistically visualize an arbitrary 3D scene by recreating some of the 3D visual cues. Cues that are recreated depend on the capability of the display. The most advanced ones, the light field displays, aim at reconstructing the underlying light field and thereby recreating most of the visual cues and consequently reproducing the most complete version of the 3D scene.

Though the light field display technology made significant advances over the last three decades, the currently existing displays still have considerable technological limitations. Those are manifested mainly in terms of finite number of light rays that a display is capable of reproducing. This limitation imposes finite spatial and angular display resolutions which in turn limits the smallest spatial feature the display can visualize as well as the depth range which can be reproduced on the display without artifacts [1]. These artifacts can be interpreted as aliasing when a display is considered as a discrete system with finite bandwidth that is sampling and reconstructing a light field describing a 3D scene with theoretically unlimited bandwidth. To remove aliasing, based on the sampling theory, before visualization on the display, the input light field must be band limited, that is, filtered to the bandwidth supported by the display. A proper filtering will remove or blur all details in the scene that the display cannot reproduce, resulting in a more appealing visualization.

In the case of automultiscopic 3D displays, Zwicker et al. [2], proposed a method for the antialiasing of a sparsely sampled light field. In their approach, the acquired light field is first reconstructed, then reparametrized and filtered with a resampling filter that is based on the display's bandwidth. The aim of the approach is to blur angular frequencies that the automultiscopic 3D display cannot reconstruct. In a more general case, Isaksen et al. [3], proposed a dynamic reparameterization for light fields by novel view synthesis with weighted averaging over an aperture in a moderately sampled light field, which acts as a low-pass filter and eliminates content that cannot be reconstructed without aliasing. However, the authors are not aware of any prior research proposing an approach to tackle the aliasing issue in projection-based light field displays.

In this paper, we propose two (antialiasing) filtering methods for projection-based light field displays which aim at matching the input light field data with the available depth budget of the display, thus, reducing or eliminating aliasing. We also discuss the pros and cons of each antialiasing method by visualizing results on a projection-based light field display.

This paper is organized as follows: Section 2 introduces the basic light field concepts utilized in this paper. The proposed methodology for antialiasing filtering is presented in Section 3. The experimental results are given in Section 4, and the concluding remarks are summarized in Section 5.

II. BACKGROUND

A. Light Field Parameterization

In this paper, we use the two-plane parameterization $L(s,t,u,v)$ to represent a light field [4]. As illustrated in Figure 1, the st-plane and the uv-plane are the camera and the image plane, respectively. Furthermore, $L(s_0,t_0,u,v)$ is also referred to as a (camera) view. For a constant s, that is, $s=s_0$, the full parallax (FP) light field $L(s,t,u,v)$ is reduced to a 3D light field $L_{s_0}(t,u,v)=L(s_0,t,u,v)$, referred to as a horizontal parallax only (HPO) light field.

Light field representation can be further simplified by introducing the concept of epi-polar plane images (EPIs). An EPI from a light field $L(s,t,u,v)$ is obtained by fixing $(s,u)=(s_0,u_0)$ or $(t,v)=(t_0,v_0)$ resulting in horizontal $E_{s_0,u_0}(t,v)=L(s_0,t,u_0,v)$ or $E_{t_0,v_0}(s,u)=L(s,t_0,u,v_0)$ vertical EPI, respectively. The neat concept behind EPI is that each point in space is mapped to a line in EPI, and

consequently, all points at the same depth are mapped to the same angle in EPI spectrum. Example of an EPI in the spatial and frequency domain is given in Figure 2.

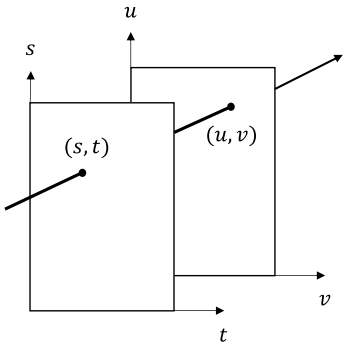

Figure 1. Two-plane light field parameterization.

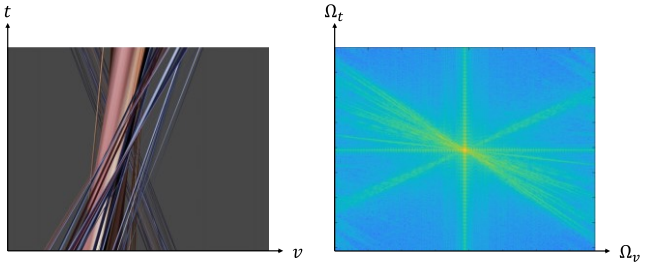

Figure 2. Epipolar plane image (EPI) $E_{s_0,u_0}(t,v)$. (a) Spatial domain. (b) Frequency domain.

The sampling density on the st- and uv-planes determines the sparsity of the light field. If for a given scene the density is such that the maximum distance of a point in the uv-plane between two closest samples on the st-plane is less than one pixel (corresponds to disparity between adjacent views being less than one pixel), then the corresponding light field is referred to as a densely sampled light field (DSLF) [1]. The main advantage of a DSLF over a sparsely sampled light field (SSLF) where the disparity is larger than one pixel is that in a DSLF there is no aliasing in the corresponding frequency domain representation which in turn makes any further interpolation of the light field trivial, e.g., one can use a simple bilinear interpolation to further interpolate a DSLF. Alternatively, if only SSLF is available, it can be interpolated to the corresponding DSLF by using one of the many existing light field interpolation (reconstruction) methods, e.g., [5],[6],[7].

B. Projection-Based Light Field Displays

Projection-based light field displays consist of two main parts as depicted in Figure 3(a): a set of projectors at the projector plane that act as ray generators and an optical element (also referred to as holographic diffusor) at the screen plane which converts the display's discrete set of rays into a continuous function [8]. Projection-based displays do not have a pixel structure as rays are generated by several independent sources and the propagated rays have a regular but not rectangular sampling structure on the display's screen, see Figure 3(b) [9].

The light field display's limited spatial and angular resolution causes a reduction in effective spatial resolution proportionally to the distance of the visualized object from the displays' screen plane. On the display, this is visible as aliasing when visualizing light field content that fails outside of the display's depth budget. There are two approaches to estimate the depth budget of the display, that is, its spatial and angular resolution. First approach is analytical and was described in [9]. Second approach is based on subjective and objective measurements and was described in [10]. In this work, we use the bandwidth estimation obtained from the analytical approach.

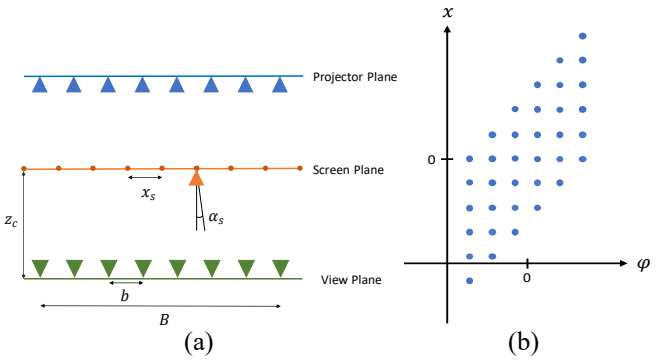

Figure 3. Projection-based light field display. (a) Physical setup. (b) Example of a possible sampling pattern at the screen plane.

III. METHODOLOGY

In this paper we propose two methods for reducing aliasing errors in projection-based light field displays. Both share the same pipeline, as illustrated in Figure 4. In both cases, our starting point for performing antialiasing filtering is a DSLF of a desired scene captured or rendered by parallel equidistant cameras (FP for Method 1 and FP or HPO for Method 2).

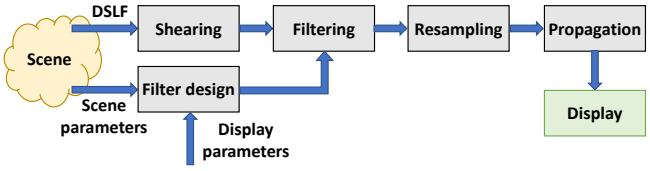

Figure 4. The proposed antialiasing methodology pipeline.

In both proposed methods, the first step is to shear the input DSLF to the screen plane. The amount of shear depends on the sampling rate on st- and uv- planes of the DSLF and the distance between the camera plane and the screen plane. The amount of shear in pixels between adjacent views can be evaluated as

$$shear = \frac{fb}{z_c},$$

where f is the focal length in pixels, z_c is the distance to the display and b is the distance between adjacent views, c.f. Figure 3(a). Here, we assume that b is the same in horizontal and vertical direction. Such shearing will recenter the DSLF to the screen plane, which means that the disparity of all points on the screen plane will be zero.

The design of the antialiasing filter depends on the sampling density of the DSLF (scene parameters) and the display bandwidth (display parameters). In Method 1, a circular filter is designed with the impulse response being

$$h_{s_0,t_0}(s,t) = \begin{cases} 1 & \text{for } \sqrt{(s-s_0)^2 + (t-t_0)^2} \le r \\ 0 & \text{otherwise} \end{cases},$$

with $r = \lceil d/2 \rceil$ and d being the decimation (resampling) factor from the DSLF sampling rate to the display's screen sampling rate evaluated as

$$d = \left\lfloor \frac{\alpha_s}{\tan^{-1}(b/z_c)} \right\rfloor,$$

with α_s being the angular resolution of the projection-based light field display. For creating the filtered view $L_f(s_0, t_0, u, v)$, at every position $(s_0, t_0) \in (s, t)$, one has to sum-up all views on positions (s, t) around (s_0, t_0) in radius r, that is,

$$L_f(s_0, t_0, u, v) = \frac{1}{M} \sum_s \sum_t h_{s_0,t_0}(s,t)\, L(s,t,u,v)\,,$$

where the normalization factor $M = \sum_s \sum_t h_{s_0,t_0}(s,t)$ is the number of contributing views. This filtering is equivalent to sensing the scene from position (s_0, t_0) with a camera lens having aperture diameter $2r$, as illustrated in Figure 5. Therefore, we also refer to this method as aperture filtering.

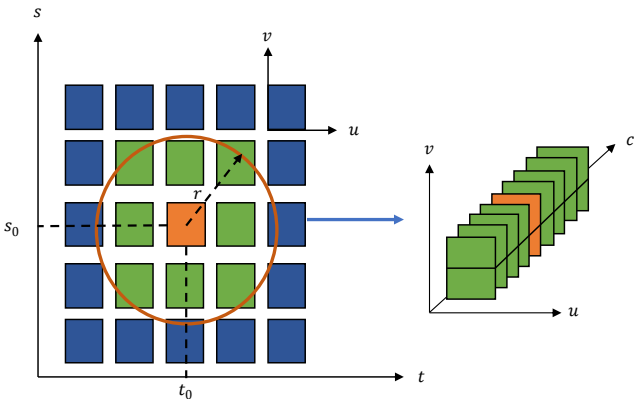

Figure 5. Illustration of averaging over viewpoints that reside in a circular proximity (aperture) of radius r (Method 1).

In Method 2, the antialiasing is done by filtering the DSLF in EPI domain. The impulse-response coefficients of the applied filters can be considered as non-uniform weights over a finite number of adjacent views. In this paper, we used windowing technique with the Gaussian window to design a filter with impulse response $h(n, f_c)$ as follows:

$$h(n, f_c) = w_{gauss}(n) h_{id}(n, f_c) \text{ for } -\frac{N}{2} \le n \le \frac{N}{2},$$

where $w_{gauss}(n)$ is the Gaussian window function defined as

$$w_{gauss}(n) = \begin{cases} e^{-\frac{1}{2}\left(\beta \frac{n}{\frac{N-1}{2}}\right)^2} & \text{for } -\frac{N-1}{2} \le n \le \frac{N-1}{2} \\ 0 & \text{otherwise,} \end{cases}$$

and $h_{id}(n, f_c)$ is the impulse response of the ideal sinc filter

$$h_{id}(n, f_c) = \begin{cases} 2f_c sinc(2\pi n f_c) & \text{for } n \neq 0 \\ 2f_c & \text{for } n = 0, \end{cases}$$

with cutoff frequency being

$$f_c = \frac{1}{d}.$$

The filter order N must be at least larger than or equal to the decimation factor d but should be preferably larger, e.g., $N \ge 2d$, to obtain a good filtering performance. Moreover, the Gaussian window width factor β should be selected such that the values of the window approach zero towards its edges.

For creating the filtered view on the position (s_0, t_0), we filter successively each horizontal and vertical EPI as

$$E^{(h)}_{s_0,u_0}(t, v_0) = E_{s_0,u_0}(t, v_0) * h_h(t, f_c) \text{ for } \forall v_0 \in v$$

$$E^{(v)}_{t_0,v_0}(s, u_0) = E^{(h)}_{t_0,v_0}(s, u_0) * h_v(s, f_c) \text{ for } \forall u_0 \in u,$$

where $h_h(t, f_c)$ and $h_v(s, f_c)$ are the horizontal and vertical impulse response and '*' is the convolution operator. As in Method 1, this must be repeated for every $(s_0, t_0) \in (s, t)$. The filtered light field $L_f(s, t, u, v)$ is a combination of all filtered EPIs for all s's and t's. As it will be illustrated in Section IV, in many cases, filtering only in horizontal direction (over HPO DSLF) produces satisfactory results when visualizing the scene on an HPO light field display.

For the sake of brevity, we assumed that the sampling on the uv-plane is the same for the input DSLF and the display. If this is not the case than additional resampling is needed also on the uv-plane. This can be done by any of the standard image down-sampling algorithms.

Afterward, the filtered light field $L_f(s, t, u, v)$ is resampled to the display grid. This can be done by a bilinear interpolation. The resampled light field is then back propagated to the ray generator plane and can be finally visualized on the display.

Though both proposed methods follow similar pipeline, the fundamental difference between them is the motivation behind the filter design (filtering). Method 1 is inspired by the working principle of a camera lens and the designed filter behaves as a lens aperture. As such, the result obtained by Method 1 can be considered as the best achievable visual performance on a display with finite bandwidth. Method 2 is inspired by signal processing, where a desired bandwidth in the frequency domain can be achieved by a proper antialiasing filter design. Method 2 can be applied on both HPO and FP DSLF, it requires less time and memory complexity because FIR filters can be applied separately in horizontal and vertical direction, and still produces similar visual quality like Method 1. In addition, filtering HPO DSLF is faster because it needs fewer views for rendering and filtering.

IV. EXPERIMENTS

The starting point in our methods is a DSLF. As we have not found publicly available FP DSLF with a large depth range, in this paper, Blender [11] is used as a 3D rendering engine to render synthetic FP DSLFs. By working with synthetic rendered scenes, we avoid potential issues that can arise when capturing real scenes (e.g., due to camera imperfection) and focus only on the aliasing issues that are discussed in the paper. We rendered three FP DSLFs from three different scenes. The scene specific rendering parameters are given in TABLE I. The resolution of the rendered images is 1280x720, the sensor width of the pinhole camera is 32 mm, and the distance to the screen of the display is $z_c = 3000$ mm. For visualization of the 3D content, we used Holografika's

Holovizio 722RC projection-based light field display [12], with screen dimension 1560 mm by 880 mm. Based on the evaluation in [9], this displays horizontal and angular sampling rate on the screen plane is $(x_s, \alpha_s) \approx (1\text{mm}, 1°)$. Moreover, without loss of generality, the shearing step in the proposed pipeline is implemented during the DSLF rendering stage in Blender. Since the target display is an HPO light field display, we need only one horizontal row as input to the display, that is, $L_{s_0}(t, u, v)$. Therefore, the number of rows that need to be rendered in a FP DSLF is equal to the filter size along the vertical (s) dimension.

All selected scenes contain features with different size and have a depth range that is considerably larger than the display's depth budget. The central rendered views are shown in Figure 7. Figure 8 shows the visualization of the rendered scenes with and without proposed antialiasing filters on the used projection-based light field display. Without filtering, c.f. Figure 8(a), large aliasing artifacts are noticeable on areas that contain small features and are far from the screen plane (e.g., zoomed in areas marked with white rectangles). As illustrated in Figure 8(b)-(d), after processing the rendered DSLF with proposed methods, regions out of display's depth budget which causes aliasing are blurred. However, regions residing in the display's depth budget stay sharp (e.g., zoomed in areas marked with yellow rectangles). The difference between applying filters on HPO and FP DSLF is visualized in Figure 6. The figure shows that filtering HPO DSLF doesn't blur horizontal dominant features. Since filtering HPO DSLF is faster than filtering FP DSLF or aperture filtering (e.g., fewer views need to be rendered and filtered), this solution might be, in some cases, considered acceptable. Furthermore, aperture filtering and filtering the FP DSLF creates similar result as both methods similarly blur features in both horizontal and vertical direction. Finally, as a large number of vertical rows in an FP DSLF drastically increases the rendering time, we opted to use a filter order in FP DSLF that is smaller than in the case when filtering an HPO DSLF. Such smaller order results with filters that have a wider transition band. Nevertheless, as seen in Figure 8, results show that utilized antialiasing approaches successfully reduce the aliasing artifacts. This demonstrated that filtering in vertical direction is less problematic when visualizing the result on an HPO light field. All filter parameters used for designing the filters are given in TABLE II.

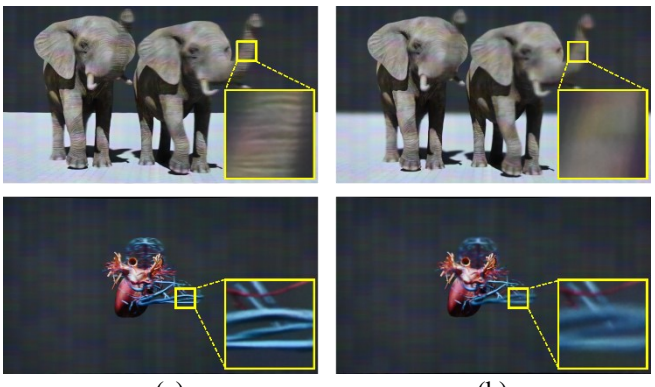

(a) (b)

Figure 6. The comparison between applying filters on (a) HPO and (b) FP DSLF.

TABLE I SCENE SPECIFIC CAPTURE PARAMETERS.

Parameter	Value		
	Vessels	Elephant	Trunk
Horizontal baseline B [mm]	2640	2000	1320
Distance between adjacent views on st-plane b [mm]	4	3	2
Minimum distance to the scene z_{min} [mm]	2300	2150	1900
Number of rendered horizontal views C_t	661	667	661
Number of rendered vertical views C_s	27	35	53

TABLE II SCENE SPECIFIC FILTER PARAMETERS.

Parameter	Value		
	Vessels	Elephant	Trunk
Decimation factor d	13	17	26
Aperture radius r	7	9	13
Filter order for FP DSLF	26	34	52
Filter order for HPO DSLF	52	68	104
Gaussian window width factor β	2	2	2

V. CONCLUDING REMARKS

In this paper we proposed and demonstrated the effectiveness of two methods for antialiasing a DSLF with the aim to improve the visual quality when reproducing the light field on a projection-based light field display. The first method applies a uniform circular filter on a FP DSLF, which mimics a camera lens. The second method applies 1D FIR low-pass filters on HPO/FP DSLF with the aim to properly filter the DSLF before downsampling it to the display's sampling grid. By visualizing the filtered light fields on a projection-based light field display, we have shown that the aliasing artifacts generated on the display have been mitigated.

Though both proposed methods are good in reducing the aliasing artifacts, there are several limitations of the proposed methods that could be further improved. First, both methods require a DSLF as input which is challenging to capture or time-consuming to render. Second, both methods are too slow to be used in real-time applications, with Method 1 requiring more time and memory than Method 2 due to 2D filtering applied over FP DSLF. As such, one direction for future work would be to develop methods that would achieve a similar visual quality faster. Third, though the improvements in the visual quality after filtering are obvious, as seen in Figure 8, it would be also interesting to confirm this by subjective studies. Furthermore, by means of subjective studies one could also evaluate how much blurriness vs aliasing users prefer and/or tolerate. This would enable one to choose the filters that match user expectations.

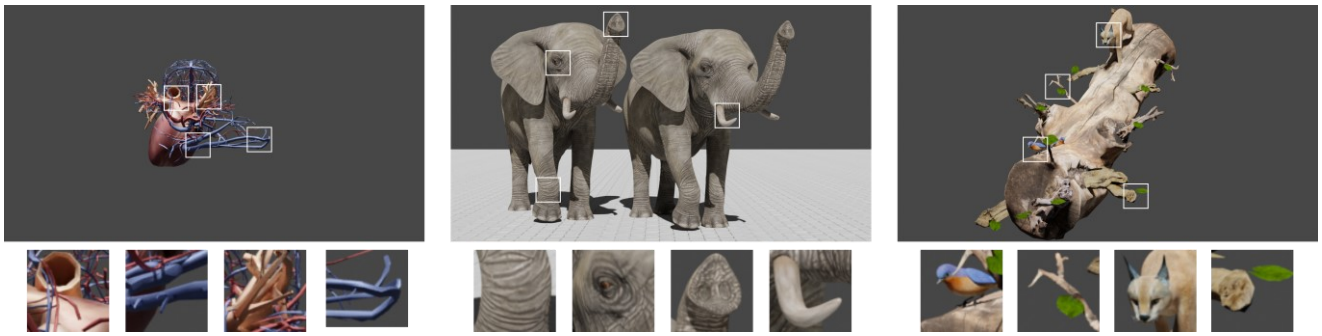

(a) (b) (c)

Figure 7. Central rendered view for scenes under consideration. (a) Vessels. (b) Elephant. (c) Trunk.

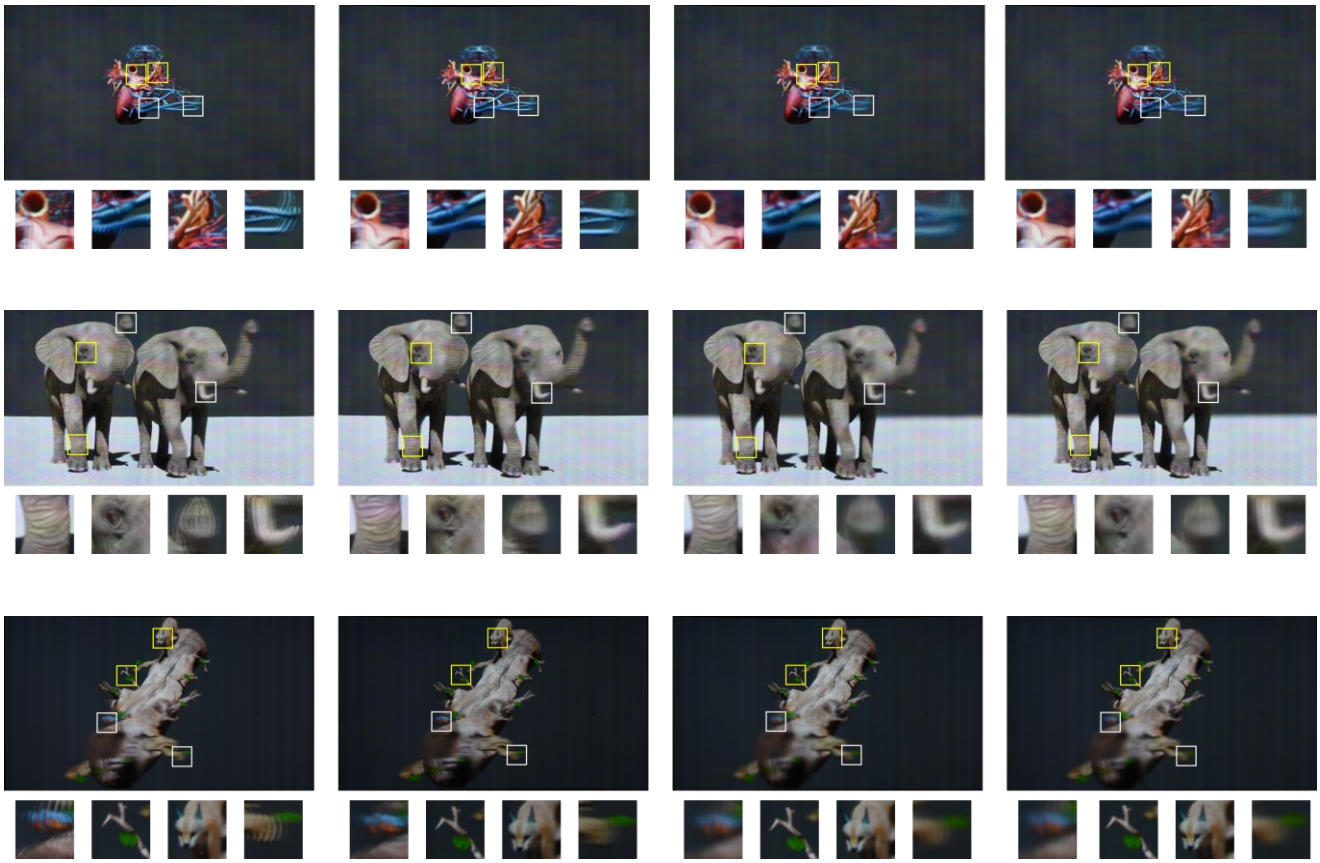

(a) (b) (c) (d)

Figure 8. Visualization of the scenes on Holovizio 722RC light field display: (a) Original. (b) EPI filtered on HPO DSLF (Method 2). (c) EPI filtered on FP DSLF (Method 2). (d) Aperture filtered (Method 1). Rectangles with yellow and white outline show regions inside and outside of the display's depth budget, respectively.

VI. REFERENCES

[1] R. Bregović, E. Sahin, S. Vagharshakyan, A. Gotchev, “Signal processing methods for light field displays,” *Handbook of Signal Processing Systems, 2nd edition*, S. Bhattacharyya, E. Deprettere, R. Leupers, and J. Takala, eds., Springer, pp. 3–50, 2019. doi: 10.1007/978-3-319-91734-4 1

[2] M. Zwicker, W. Matusik, F. Durand, H. Pfister, “Antialiasing for automultiscopic 3D displays”, *Proc. of Eurographics Symposium on Rendering*, 10 pages, 2006. doi: 10.1364/AO.52.000D97

[3] A. Isaksen, L. McMillan, S. J. Gortler,” Dynamic reparameterized light fields,” *Proc. Conference on Computer Graphics and Interactive Techniques (SIGGRAPH)*, pp. 297-306, 2000. doi: 10.1145/344779.344929

[4] M. Levoy, P. Hanrahan, “Light field rendering,” *Proc. of Computer Graphics (SIGGRAPH)*, pp. 31-42, 1996. doi: 10.1145/237170.237199

[5] S. Vagharshakyan, R. Bregović, and A. Gotchev, “Light field reconstruction using shearlet transform,” *IEEE Trans. on Pattern Analysis and Machine Intelligence*, vol. 40, no.1, pp. 133-147, 2018. doi: 10.1109/TPAMI.2017.2653101

[6] T. Hu, L. Shu, C. Yilun, S. Tiancheng, J. Jiaya, ”EfficientNeRF: Efficient Neural Radiance Fields,” *arXiv*, July 2022. doi: 10.48550/arXiv.2206.00878

[7] G. Wu, Y. Liu, L. Fang and T. Chai, "Revisiting Light Field Rendering with Deep Anti-Aliasing Neural Network," in IEEE Transactions on Pattern Analysis and Machine Intelligence, vol. 44, no. 9, pp. 5430-5444, 1 Sept. 2022. doi: 10.48550/arXiv.2104.06797

[8] T. Balogh, “The HoloVizio system,” *Proc. SPIE 6055*, 2006. doi: 10.1117/12.650907

[9] R. Bregović, P. T. Kovács, and A. Gotchev, “Optimization of light field display-camera configuration based on display properties in spectral domain,” *Opt. Express*, vol. 24, no. 3, pp. 3067-3088, 2016. doi: 10.1364/OE.24.003067

[10] P. T. Kovács, R. Bregović, A. Boev, A. Barsi, and A. Gotchev, “Quantifying spatial and angular resolution of 3D light-field displays,” *IEEE Journal of Selected Topics in Signal Processing*, vol. 11, no. 7, pp. 1213-1222, Oct. 2017. doi: 10.1109/JSTSP.2017.2738606

[11] B. O. Community, Blender - a 3D modelling and rendering package, Stichting Blender Foundation, Amsterdam, 2018. URL: http://www.blender.org , accessed 16.05.2023.

[12] “HoloVizio 722RC Large-scale 3D display,” https://holografika.com/722rc/ , accessed 16.05.2023.